An Alternative Method for Characterization and Comparison of Plant Root Shapes

A thesis submitted to the
College of Graduate and Postdoctoral Studies
in partial pulfillment of the requirements
for the degree of Master of Science
in the Department of School of Environment and Sustainability
University of Saskatchewan
Saskatoon

By
Yujie Pei

Contents

[Yuge 1] Please revise this

[Yuge 2] Dave, Please give me the feedback or comments on this subsection.

Existed Morphological Descriptors for Root Systems

An Alternatively Mathematical Method for Shape Description

2.1 Heat Content in Annulus

Since the heat equation, also known as the diffusion equation, defined in an annulus possesses explicit solutions, the analytical expressions of heat content, derived by the integration over the whole domain, are then accessible. In this section, the preliminary step is to solve the initial-boundary value problem (IBVP) defined in the annulus. As the solution of IBVP and its related quantities are in the form of the infinite series, the numerical method will be used to approximate them to validate the research methodology in the next chapter.

2.1.1 Analytical Results

[Yuge 3] Please revise this

The 2-dimensional heat equation [7] Eq. 2.1 defined in the polar coordinate system describes the heat distribution or temperature varying in time and positions in the domain Ω shown in Figure 2.1. $u(r, \theta, t)$ is the unknown function to be solved, where r is radial coordinate, θ is the angular coordinate, and t is the time. D is the diffusion coefficient and determines how fast u changes in time.

$$u_t = D(u_{rr} + \frac{1}{r}u_r + \frac{1}{r^2}u_{\theta\theta}) \tag{2.1}$$

$$u = 0 \quad on\ \partial\Omega_1 \tag{2.2}$$

$$u' = 0 \quad on\ \partial\Omega_2 \tag{2.3}$$

$$u(r, \theta, 0) = \frac{1}{|\Omega|} \tag{2.4}$$

From the microscopic and probabilistic perspective, $u(r, \theta, t)$ is a probability density function, which gives the value of heat particles at (r, θ) at time t. Eq. 2.2 and Eq. 2.3 are the homogenous Dirichlet boundary condition and the homogenous Neumann boundary condition, respectively. In other words, the inner boundary $\partial\Omega_1$ is cooled to the zero temperature because the heat particles will be absorbed when they encounter $\partial\Omega_1$. The outer boundary $\partial\Omega_2$ is perfectly insulated since the heat particles will be reflecting when they reach $\partial\Omega_2$. Eq. 2.4 states that the heat particles distribute uniformly over the whole domain at time $t = 0$, where $|\Omega|$ equals the total area of the annulus.

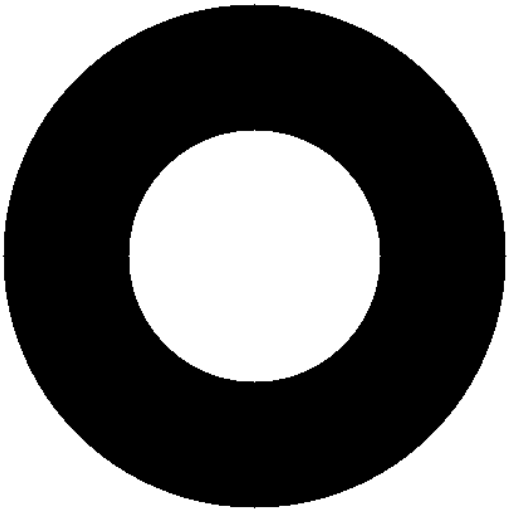

Figure 2.1: Assume the annulus Ω is a homogeneous and isotropic medium and has the inner boundary $\partial\Omega_1$ with radius a and outer boundary $\partial\Omega_2$ with radius b.

Solving Heat Equation

Generally, before solving the heat equation, it is convenient and efficient to generate a group of dimensionless variables by dimensional analysis. The benefit of dimensional analysis is that many physical parameters can be combined into a smaller number of unitless variables, which do not depend on the unit of the measurements and can also describe the phenomenon or system of interest [2].

Let $\mu = b/a$ be the dimensionless radius ratio, $\tau = \frac{Dt}{a^2}$ be the dimensionless time, and $\hat{r} = \frac{r}{a}$ be the unitless radius. Substitute these dimensionless variables into Eq. 2.1 and rewrite it as

$$u_\tau = (u_{\hat{r}\hat{r}} + \frac{1}{\hat{r}}u_{\hat{r}} + \frac{1}{\hat{r}^2}u_{\theta\theta}) \tag{2.5}$$

With the uniform initial condition,

$$u(\hat{r}, \theta, 0) = \frac{1}{|\Omega|} \tag{2.6}$$

With the homogenous boundary conditions

$$u(1, \theta, \tau) = 0 \tag{2.7}$$

$$u'(\mu, \theta, \tau) = 0 \tag{2.8}$$

After implementing the separation of variables method [7], the solutions of Eq. 2.5 with conditions Eq. 2.6, Eq. 2.7, and Eq. 2.8 are

$$u(\hat{r},\theta,\tau)=\sum_{n=1}^{\infty}\tilde{c_{0,n}}\left\{J_0(\sqrt{\lambda_{0,n}})Y_0(\sqrt{\lambda_{0,n}}\hat{r})-Y_0(\sqrt{\lambda_{0,n}})J_0(\sqrt{\lambda_{0,n}}\hat{r})\right\}e^{-\lambda_{0,n}\tau} \tag{2.9}$$

where

$$\tilde{c_{0,n}}=\frac{1}{(\mu^2-1)}\frac{1}{\left[\frac{J_0(\sqrt{\lambda_{0,n}})}{J_0'(\mu\sqrt{\lambda_{0,n}})}\right]^2-1} \tag{2.10}$$

Eigenvalues $\lambda_{0,n}$ ($n\in\mathbb{N}_+$) appeared in Eq. 2.9 and Eq. 2.10 is the nth positive root of the eigenfunction Eq. 2.11, which is a cross-product of the Bessel function [19]

$$F_0(\lambda)=J_0(\sqrt{\lambda})Y_0'(\sqrt{\lambda}\mu)-J_0'(\sqrt{\lambda}\mu)Y_0(\sqrt{\lambda}) \tag{2.11}$$

Heat Content (Survival Probability)

The amount of heat contained in Ω at the moment $\tau>0$ defined as heat content $Q_\Omega(\tau)$, which is an alternative terminology of survival probability $S(\tau)$ in some mathematical literatures [3] [16] [12]. $S(\tau)$ is proportional to $Q_\Omega(\tau)$ [14], which gives the probability of the particles remain diffusing in the domain Ω at time $\tau>0$ [1]. Survival probability can be expressed by

$$\begin{aligned}S(\tau)&=\int_0^{2\pi}d\theta\int_1^{\mu}\hat{r}d\hat{r}u(\hat{r},\theta,\tau)\\&=\sum_{n=1}^{\infty}\frac{4}{\mu^2-1}\frac{1}{\lambda_{0,n}\left\{\left[\frac{J_0(\sqrt{\lambda_{0,n}})}{J_0'(\mu\sqrt{\lambda_{0,n}})}\right]^2-1\right\}}e^{-\lambda_{0,n}\tau}\end{aligned} \tag{2.12}$$

Eq. 2.12 reveals some basic properties of $S(\tau)$. Firstly, when $\tau=0$, the survival probability is 1 since all the particles are just generated over the whole domain and not be absorbed by Ω_1. Secondly, $S(\tau)$ is a convergent series with multiexponential decay. Thirdly, $S(\tau)$ interconnects the overall geometric characteristics of Ω. For example, the decay rate of $S(\tau)$ in a short time heavily depends on the geometrical features of Ω_1, as only the particles inserted close to Ω_1 have the high probabilities of being absorbed. Finally, as the lone-time limit, $S(\tau)$ is represented by the lowest eigenvalue $\lambda_{0,1}$.

Mean First-Passage Time

The first passage phenomena play a fundamental role in stochastic processes triggered by a first-passage event [17]. In this thesis, we only focus on the stochastic evolution of $u(\hat{r},\theta,\tau)$ until the first-passage time, at which a heat particle reaches any sites of target boundary Ω_1 for the first time. Similarly, another essential first-passage-related quantity is the first-passage probability, which is a probability of the diffusing heat particles hitting a specified site or a set of sites at a specified time for the first time [15]. All the first-passage

characteristics can be expressed in terms of the first-passage probability. For example, the survival probability of heat particles at time τ calculated in the last subsection is

$$f(\tau) = -\frac{\partial S(\tau)}{\partial \tau} \tag{2.13}$$

where $f(\tau)$ is the first-passage probability to the target boundary Ω_1 at time τ regardless of particles' stop positions. By the definition, the nth moment of the exit time [15] is

$$\begin{aligned} \langle \tau^n \rangle &= \int_0^\infty \tau^n f(\tau) d\tau \\ &= -\int_0^\infty \tau^n \frac{\partial S(\tau)}{\partial \tau} d\tau \\ &= -\tau^n S(\tau)|_0^\infty + n \int_0^\infty \tau^{n-1} S(\tau) d\tau \end{aligned} \tag{2.14}$$

Substitue $n = 1$ in Eq. 2.14, the mean-first passage time $\langle \tau \rangle$, also called the average first-passage time, of heat particles implies an overall property of the system and can be expressed as

$$\begin{aligned} \langle \tau \rangle &= \int_0^\infty \tau dS \\ &= \sum_{n=1}^\infty \frac{4}{\mu^2 - 1} \frac{1}{\lambda_{0,n}^2 \left\{ \left[\frac{J_0(\sqrt{\lambda_{0,n}})}{J_0'(\mu\sqrt{\lambda_{0,n}})} \right]^2 - 1 \right\}} \end{aligned} \tag{2.15}$$

2.1.2 Numerical Approximation

[Yuge 4] Dave, Please give me the feedback or comments on this subsection.

The problem solved in the subsection 2.1.1 is defined in the continuous-space and continuous-time, and all the analytical results are in the form of the infinite series involving continuous variables, which will be approximated numerically in this subsection. Moreover, for simplicity, a specific kind of annulus, with the radius ratio $\mu = 2$, is considered.

The analytical $u(\hat{r}, \theta, \tau)$, $S(\tau)$, and $\langle\tau\rangle$ are in connection with the positive integers $\lambda_{0,n}$, so the preliminary step of the numerical evaluation is to calculate the monotonically increasing eigenvalues in Eq. 2.11. The Figure 2.2 reveals the monotonicity and periodicity of the $\lambda_{0,n}$. More precisely, the nth positive zero $\lambda_{0,n}$, as $n \to \infty$, can be bracketed in an interval $((n-1)\pi, (n+1)\pi)$ [10]. Therefore, the bisection method [18], a well-known and most reliable root finding method, is used to close in on the $\lambda_{0,n}$ by successively halving the interval until it becomes sufficiently small.

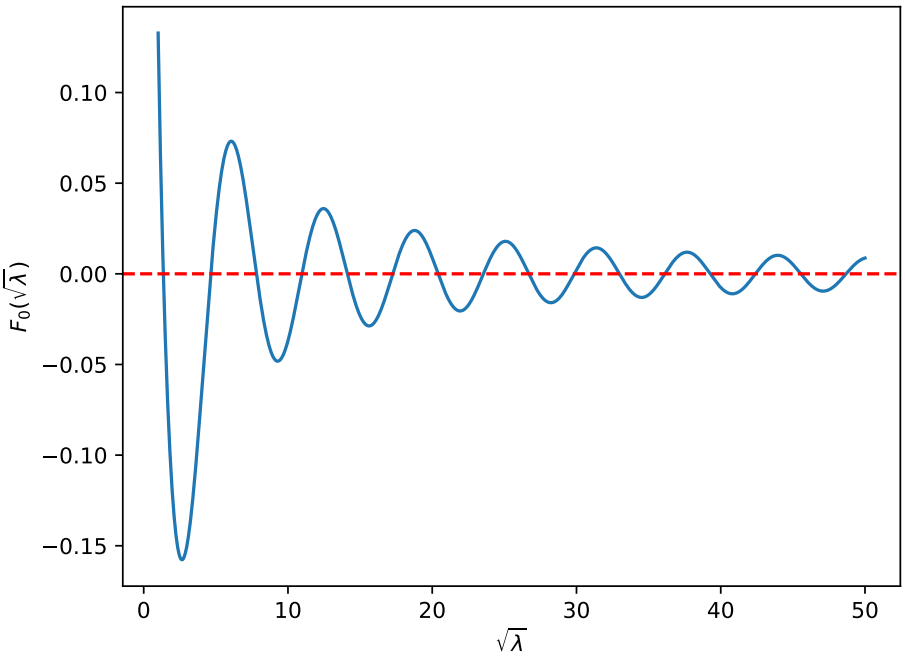

Figure 2.2: It is straightforward to evaluate the cross-product of Bessel functions Eq. 2.11 by SciPy library [18].

After the numerical estimation of the $n-$th positive root $\lambda_{0,n}$ of Eq. 2.11, the next step is to approximate $u(\hat{r}, \theta, \tau)$ with the first 1000 eigenvalues and the discretized radius $\hat{r}$ and τ. As illustrated in Figure 2.3, the diffusion problem experiences a rapid change in the very beginning, but then the evolution of u becomes slower and slower. Finally, the initial shape of u can not be recognized anymore.

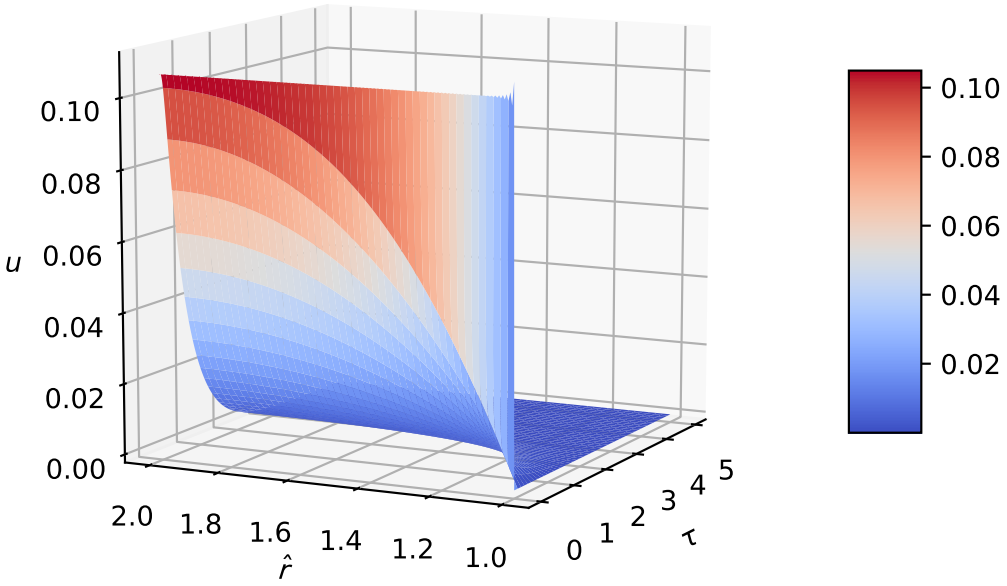

Figure 2.3: When $\tau = 0$, the approximated initial value of u is about 0.106079414 while the analytical result is $1/3\pi \approx 0.106103295$. The absolute error is 2.3881×10^{-5}. Moreover, the Gibbs phenomena [11] happened obviously near the discontinuity $\hat{r} = 0$ with the overshoots and undershoots because of the Fourier-Bessel series.

Before the numerical approximation of the convergent non-alternating general Dirichlet series [13] $S(\tau)$, $S(0)$ is evaluated firstly, and it can be represented as

$$\begin{aligned} S(0) &= \sum_{n=1}^{\infty} \frac{4}{\mu^2 - 1} \frac{1}{\lambda_{0,n} \left\{ \left[\frac{J_0(\sqrt{\lambda_{0,n}})}{J_0'(\mu\sqrt{\lambda_{0,n}})} \right]^2 - 1 \right\}} \\ &= \sum_{n=1}^{\infty} c_n \end{aligned} \tag{2.16}$$

As displayed in Figure 2.4a, the individual terms of the series Eq. 2.16 are monotonically decreasing and approach to 0. Calculating the $1000-$th partial sum directly, $S(0)$ is 0.9998649050990541 to 16 decimal places with 3 digit accuracy. However, Aitken's method can speed up the convergence rate of the partial sum sequence and improve the accuracy of the estimation by constructing a new series. Moreover, it does not matter whether the series is alternating or not. Aitken's acceleration is

$$A_n^{(1)} = s_{n+1} - \frac{(s_{n+1} - s_n)^2}{s_{n+1} - 2s_n + s_{n-1}} \tag{2.17}$$

where s_n, $n = 1, 2, 3, ...$, is the $n-$th partial sum of Eq. 2.16, and (s_{n-1}, s_n, s_{n+1}) are three successive partial sums. The process can be repeated for the further speed-up. For example, apply Eq. 2.17 on the new series $A^{(1)}$ to generate $A^{(2)}$, on the series $A^{(2)}$ to obtain $A^{(3)}$, etc.

As displayed in Figure 2.4b, instead of adding 1000 terms of Eq. 2.16 directly, the result of sequence transformation by Aitken's method is more precise, which is 0.9999812339391291 to 16 decimal places with 4 digit accuracy. The error using Aitken's acceleration is 7.2 times smaller than simply using the partial sums.

Similarly, when $\tau > 0$, estimating $S(\tau)$ and $\langle\tau\rangle$ in Eq. 2.12 by Aitken's acceleration, shown in Figure 2.5, for validating the research methodology in the next chapter.

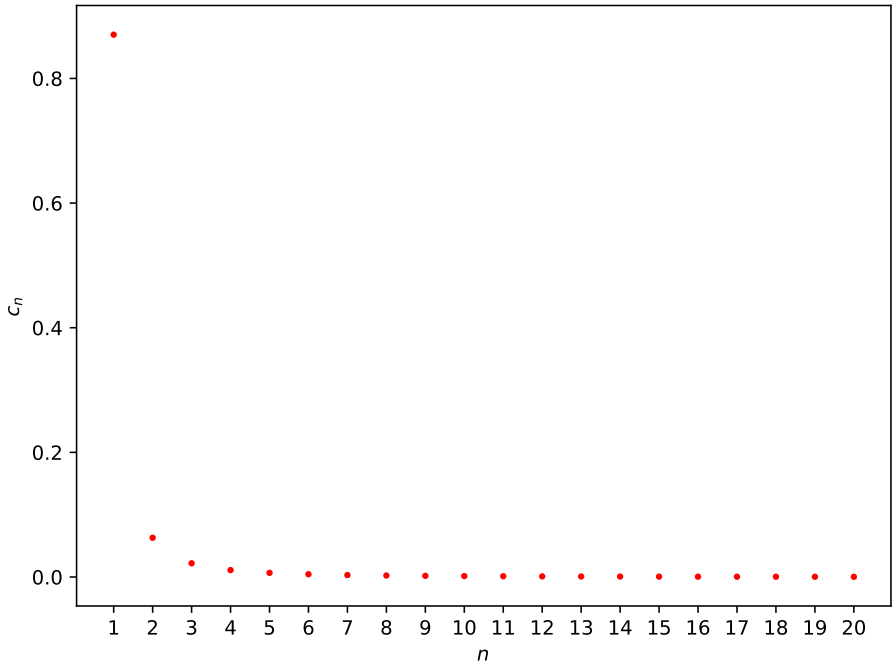

(a) The first 20 terms of the series Eq. 2.16 are convergent and tend to zero.

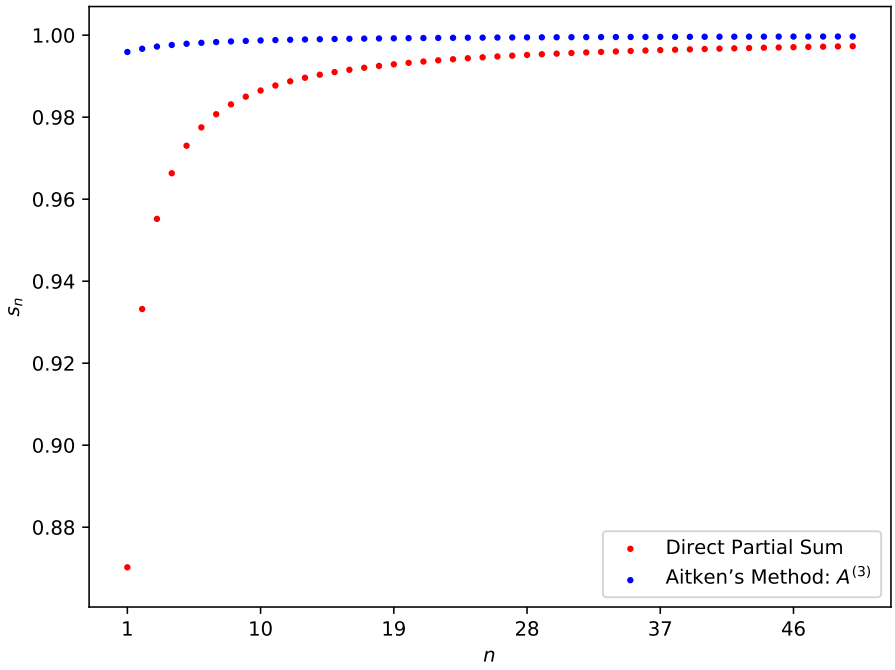

(b) The sequence of the partial sums of the series Eq. 2.16 tends to a real limit 1. Compared with calculating the sum directly, $A_n^{(3)}$ converges more rapidly and approaches closer to 1.

Figure 2.4: $S(0)$ is approximated by the direct summation and Aitken's acceleration.

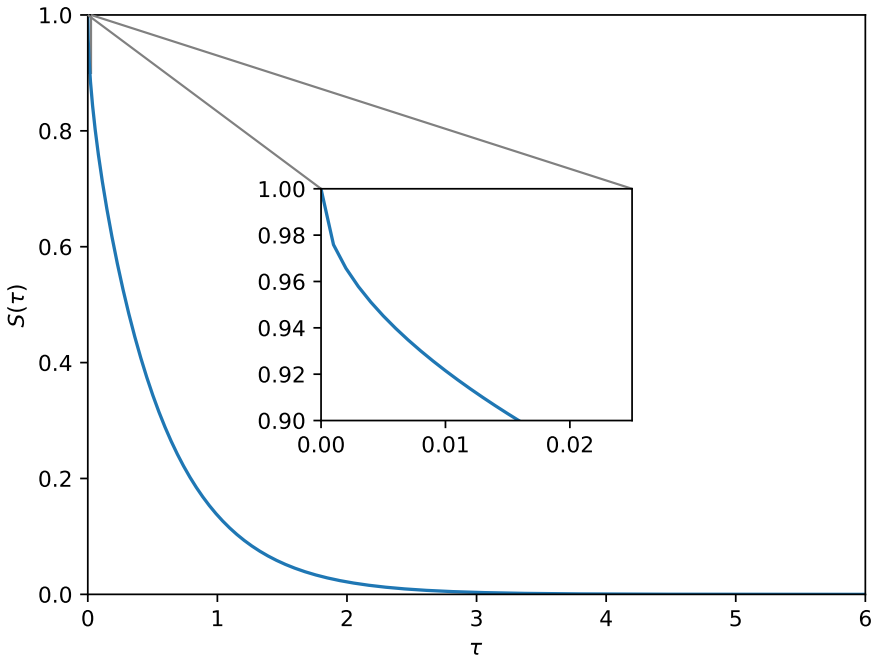

Figure 2.5: The asymptotic behaviours of survival probability $S(\tau)$ is approximated by the Aitken's acceleration. $S(\tau)$ monotonously decreases from 1 at $\tau = 0$ to 0 as τ goes to infinity. Moreover, the approximation of analytical mean first-passage time $\langle\tau\rangle$ equals 0.47339248149521174..

Fixed-time Step Monte Carlo Simulations on Artificial Images

3.1 Methodology Validation

In the last chapter, the survival probability $S(\tau)$ and the mean first-passage time has been calculated by solving the heat equation and approximated by the numerical methods. Lattice Random Walks (LRWs) and Pearson's Random Walks (PRWs) are implemented in the annulus image, as shown in Figure 2.1, in Python. This section aims to validate the research methodology by comparing the estimated survival functions $S(t)$ of the numerical data with the analytical solutions $S(\tau)$ where t is the number of steps taken by the particles in the fixed-time step Monte Carlo simulations and τ denotes the unitless time.

3.1.1 Statistical Fluctuation Analysis

Fixed-time step Monte Carlo simulations, LRWs and PRWs, are the nondeterministic numerical representations of the original statistical problem defined in the continuous-time and continuous-space with numerous inputs and discrete-time trajectories. In the simulations, the initial positions of the enormous number of particles and their moving directions at each time step are determined by the randomly uniform sampling. Thus, it is inevitable to appear the statistical fluctuations, also called variance, defined as a measure of the discrepancies between the estimate and the true solution. The brute-force way to reduce the statistical fluctuations is to increase the sample size.

The first kind of error stems from the sampling. As shown in Figure 3.1a and Figure 3.1b, the larger sample size in the simulations, the estimated survival functions will be more precise. LRWs are used to mimic the continuous-time and continuous-space diffusion process by generating the discrete random trajectories in the discrete time, which results in the time-discretization and space-discretization errors. Although PRWs is a model defined in continuous-time and continuous-space, the random paths demand much longer time simulation as shown in Figure 3.2.

3.1.2 Sample Size Determination and Evaluation

In the last chapter, two approaches used to determine the appropriate sample size in the fixed-time step Monte Carlo simulations have been proposed. One of them is based on inferential statistics [5], which infers and estimates the unknown population parameters from the sample statistics. Another one is simpler since it does not need any simulations.

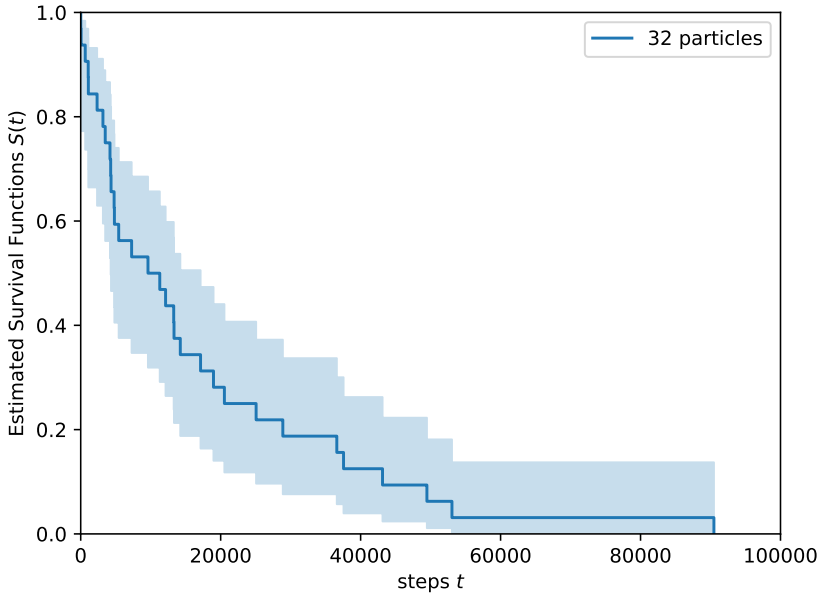

(a) Survival curve for the LRWs with 32 particles.

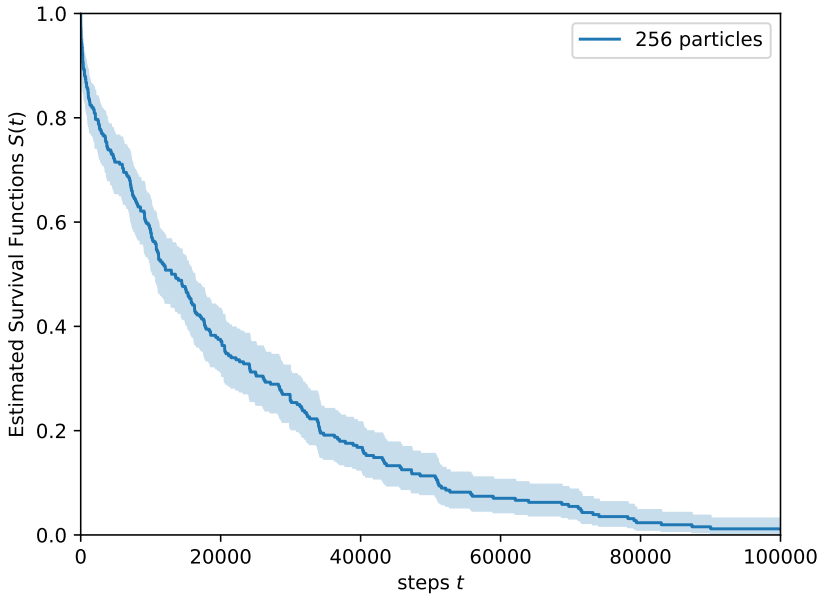

(b) Survival curve for the LRWs with 256 particles.

Figure 3.1: Estimated survival curves and 95% confidence intervals for Monte Carlo simulations of partical diffusion on an annulus. As the number of particles increasing, the uncertainty of the LRWs simulation are lower since the confidence band of the estimated survival function becomes narrower.

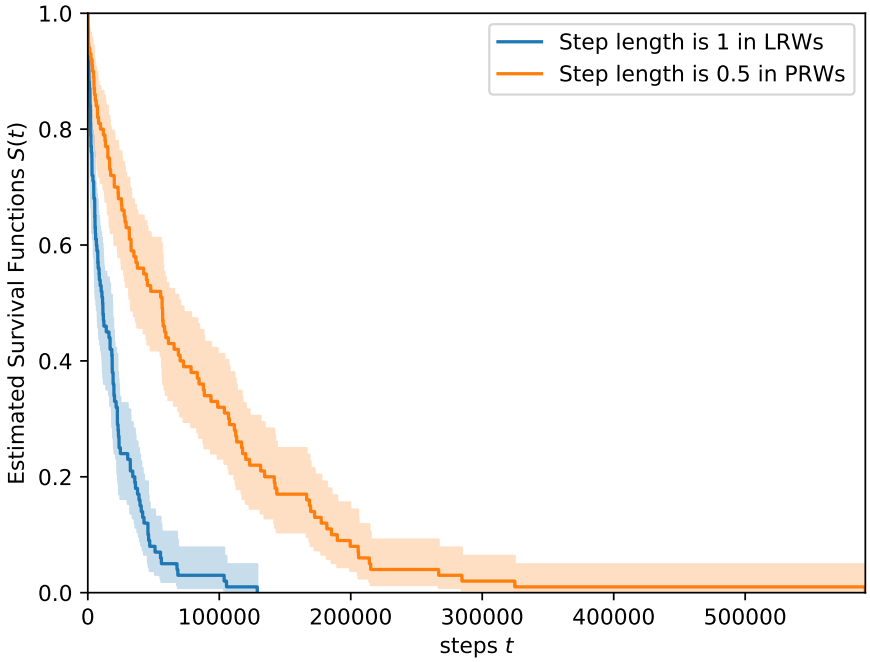

Figure 3.2: When run LRWs and PRWs in the annulus with 100 particles, the finer discretization step results in the longer simulation time.

Chebyshev's inequality

According to LLN [9], the unknown population mean first-passage time $\bar{X}$ can be estimated by sample mean $\bar{X}_N$ when N is big enough. Chebyshev's inequality [6] is a probabilistic inequality that can be applied to any probability distribution of a random variable with the finite expected value and non-zero variance. This inequality provides an upper bound to the probability that the absolute deviation of a random variable from its mean will exceed a given threshold.

In the Figure 3.3, the number of steps t in the numerical simulations have been converted into the unitless time τ by the Eq.(2.16). Thus, given a predesignated error ϵ, the required number of particles N can be determined by

[**Yuge 5**] No hard number

$$Pr(|X_N - \bar{X}| \geq \epsilon) = Pr(|X_N - \bar{X}_N| \geq \epsilon) \leq \frac{\sigma_N^2}{\epsilon^2} \approx \frac{2^b N^k}{\epsilon^2} = 0.01 \tag{3.1}$$

where $\epsilon = 0.01\bar{X}$.

The required number of particles in LRWs and PRWs can be estimated by Eq. 3.1, which is

$$N \geq (\frac{0.01\epsilon^2}{2^b})^{\frac{1}{k}} \approx 1338643 \tag{3.2}$$

where $\epsilon \approx 0.004744$, $b \approx -2.088495$, and $k \approx -0.982400$. Therefore, the number of particles should be at least 1338643 to make sure that there is no more than 1% chance of X_N to be outside $[0.46865856, 0.47812641]$.

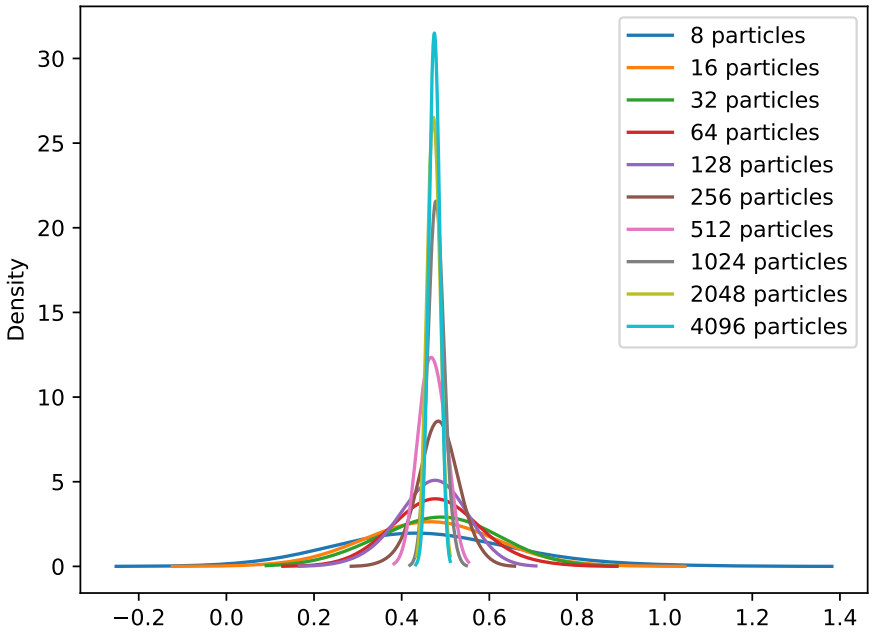

(a) Running the LRWs in the annulus with $N = 2^i$ particles and calculating the mean first-passage time X_N, where $i = 3, 4, 5, ..., 12$. For each N, replicating the simulation 50 times and recalculating the mean of the mean first-passage time $\bar{X}_N$ and the variance σ_N^2. As the sample size N increase, the distribution of the sample means X_N becomes narrower and approximately normal.

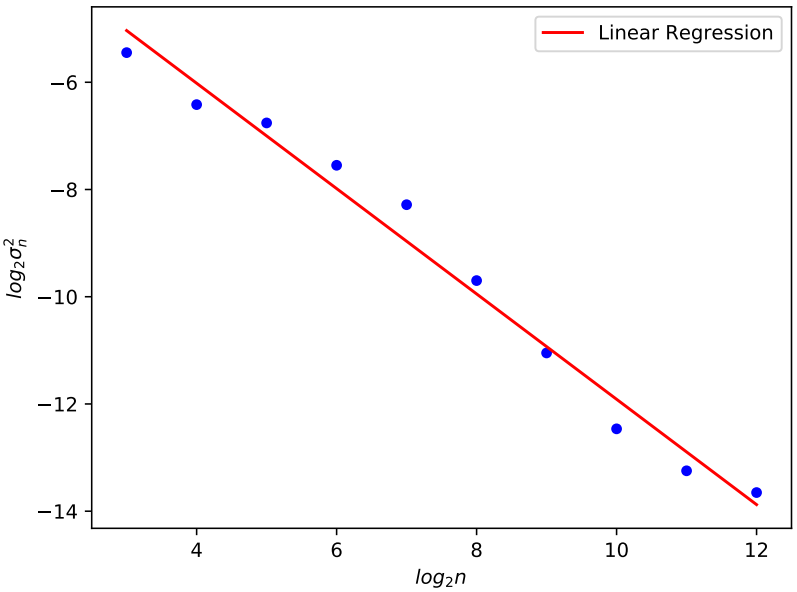

(b) A fitted linear regression model is used to explore the scaling relationship between $log_2(\sigma_N^2)$ and $log_2 N$. $log_2(\sigma_N^2) \approx b + klog_2 N$, where k and b are the estimated model parameters, slope and intercept, respectively.

Figure 3.3

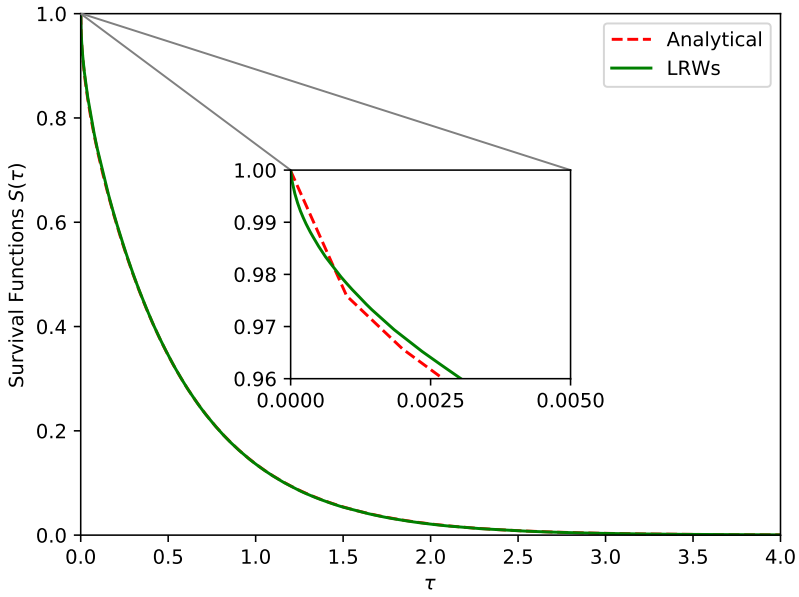

(a) Survival curve for LRWs.

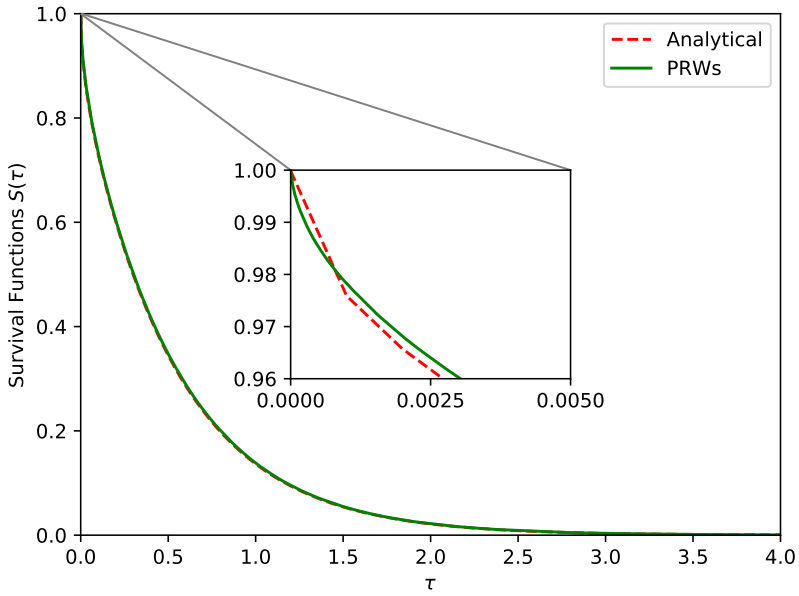

(b) Survival curve for PRWs.

Figure 3.4: Running PRWs and LRWs in the annulus with 1338643 particles determined by the Eq. 3.2 illustrating that the short and long time asypototic behaviors of the estimated survival functions of particles undergoing LRWs and PRWs are consistent with the analytical result in Eq Yuge

Test Methods (standard nonparametric)	Statistics	P Values
Logrank	0.017679	0.894223
Fleming-Harrington	0.742536	0.388850
Gehan-Breslow	0.742536	0.388850
Tarone-Ware	0.499418	0.479756

Table 3.1: The estimated survival function of 1338643 particles in the LRWs is statistically similar to the analytical survival function.

Test Methods (standard nonparametric)	Statistics	P Values
Logrank	0.039142	0.843168
Fleming-Harrington	0.083388	0.772757
Gehan-Breslow	0.083388	0.772757
Tarone-Ware	0.010582	0.918069

Table 3.2: The estimated survival function of PRWs, which has 1338643 particles with step length 0.5, is not statistically different from the analytical survival function.

From the visualized comparison in Figure 3.4 and the results of the two-sample statistical tests in Table 3.1 and Table 3.2, the fixed-step Monte Carlo simulations' results converge to the analytical outcomes. Therefore, the integral of the solutions of heat equations can be approximated by the Monte Carlo simulations without calculating manually. As mentioned in the last chapter, the integral, $S(\tau)$, indicates the annulus' geometrical information. Therefore, the fixed-time step Monte Carlo simulation can describe the shape of an object without using the rulers. However, the number of particles in the numerical simulations estimated by Eq. 3.1 is abundant, which causes a high computational cost because each random trajectories of each particle are simulated in LRWs and PRWs till they reach the inner boundary of the annulus.

Dvoretzky–Kiefer–Wolfowitz (DKW) inequality

Chebyshev's inequality can be applied to any probability distribution, but it is also weaker than other inequalities. DKW inequality is more efficient since the confidence band is generated without running any simulations. For example, let $F(\tau)$ be the true cumulative distribution function (CDF) of the first passage time, a continuous unitless random variable on the interval $[0, \infty]$. $F(\tau)$ has a relationship with $S(\tau)$, which is

$$F(\tau) = 1 - S(\tau) \tag{3.3}$$

The true CDF is known by Eq. 3.3, which can also be approximated numerically. A simple example of generating the CDF-based confidence bounds by DKW inequality is shown in Figure 3.5. The empirical distribution function $F_{256}(\tau)$ is estimated by the lifeline module in Python [8]. Thus, the interval ε contains

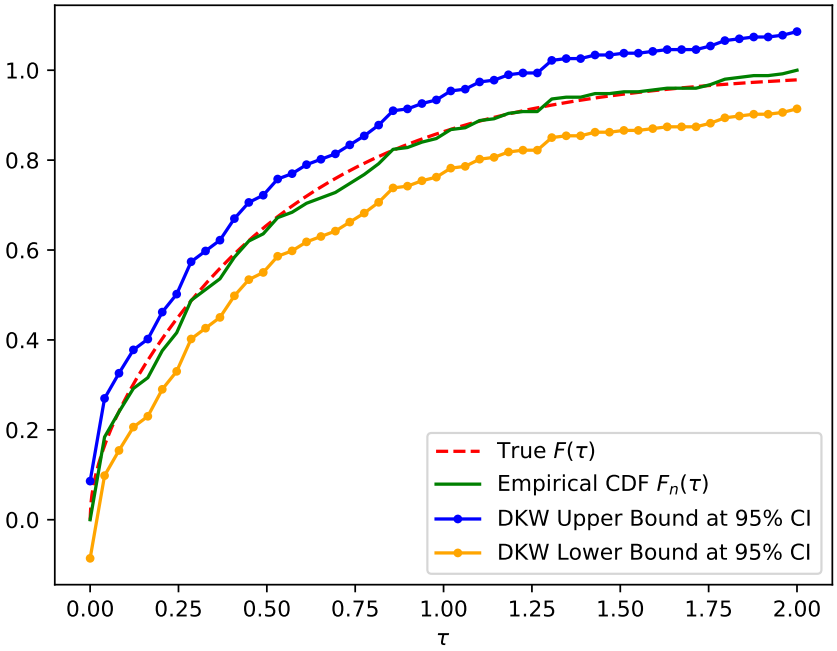

Figure 3.5: The simultaneous band around $F_{256}(\tau)$ with interval 0.084881 calculate by Eq. 3.4 encompasses the entire $F(x)$ at 95% confidence level.

the entire $F(\tau)$ with the probability 95% can be calculated by Eq.(2.20) [Yuge]

$$\varepsilon = \sqrt{\frac{\ln \frac{2}{0.05}}{2 * 256}} \approx 0.084881 \tag{3.4}$$

Moreover, the sample size estimated by DKW inequality Eq.(2.20) [Yuge] does not depend on the geometries or the kind of simulations because the simultaneous confidence bounds always contain the true cumulative distribution at a specific confidence level. For instance, assume the probability, that the maximum distance between $F_N(\tau)$ and $F(\tau)$ is bigger than 0.005, is smaller than 0.01, the minimum required number of particles should meet the inequality

$$Pr(\sup_{x \in \mathbb{R}} |F_N(\tau) - F(\tau)| > 0.005) \leq 2e^{-2N0.005^2} = 0.01 \tag{3.5}$$

Thus, after the transformation of Eq. 3.5, the sample size can be determined by

$$N \geq \frac{\ln(\frac{0.01}{2})}{-2 \times 0.005^2} \approx 105966 \tag{3.6}$$

From the Figure 3.6, Table 3.3, and Table 3.4, although the sample size in the LRWs and PRWs determined by DKW inequality is about 10 times smaller than that by Chebyshev's inequality, the estimated survival functions of the numerical simulations converge to the analytical results within the amount of statistical uncertainty.

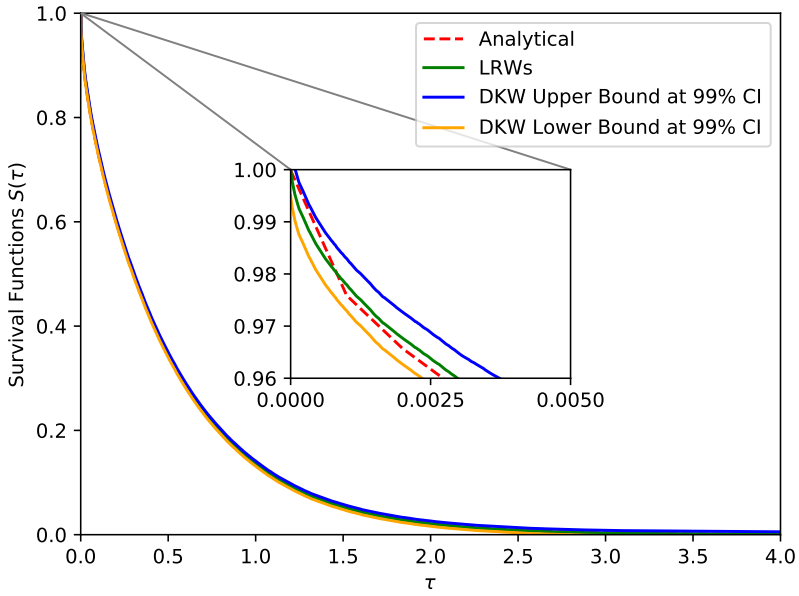

(a) The simultaneous confidence bands, generated by Eq. 3.5, of the estimated survival function $S(t)$ for LRWs contain the whole ture analytical $S(\tau)$.

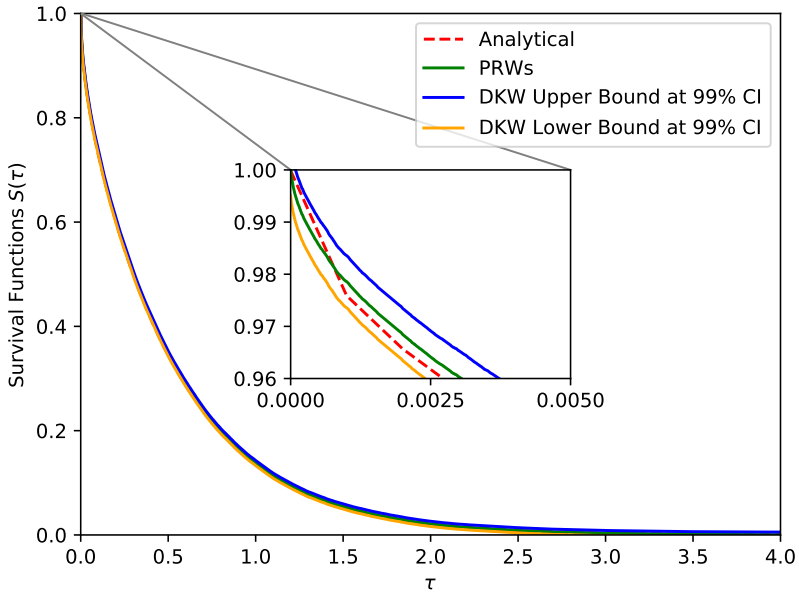

(b) The simultaneous confidence bands, generated by Eq. 3.5, of the estimated survival function $S(t)$ for PRWs contain the whole ture analytical $S(\tau)$.

Figure 3.6: PRWs and LRWs are implemented in the annulus with 105966 particles determined by the Eq. 3.6. (a) and (b) show that the DKW simultaneous confidence bands of estimated survival function with the interval 0.005 encompass the entire analytical $S(\tau)$ at 99% confidence level.

Test Methods (standard nonparametric)	Statistics	P Values
Logrank	1.532224	0.215779
Fleming-Harrington	1.630358	0.201654
Gehan-Breslow	1.630358	0.201654
Tarone-Ware	1.619530	0.203157

Table 3.3: The estimated survival function of 105966 particles in the LRWs is not statistically different to the analytical survival function.

Test Methods (standard nonparametric)	Statistics	P Values
Logrank	2.645624	0.103835
Fleming-Harrington	1.473674	0.224767
Gehan-Breslow	1.473674	0.224767
Tarone-Ware	1.986810	0.158675

Table 3.4: The estimated survival function of PRWs, which has 105966 particles with step length 0.5, is statistically similar to the analytical survival function.

3.1.3 Conclusion

Instead of calculating the asymptotic expansion of the heat content manually as $\tau \to 0^+$, the total heat energy β [12] for time $\tau > 0$ can be approximated by the fixed-time step Monte Carlo simulations for describing the full-scale geometrical features of the annulus. Moreover, the required number of particles in the simulations determined by the DKW inequality is much smaller than the superabundant value estimated by Chebyshev's inequality.

References

[1] Odd Aalen, Ornulf Borgan, and Hakon Gjessing. *Survival and event history analysis: a process point of view*. Springer Science & Business Media, 2008.

[2] Grigory Isaakovich Barenblatt, Grigorii Isaakovĭc Barenblatt, and Barenblatt Grigory Isaakovich. *Scaling, self-similarity, and intermediate asymptotics: dimensional analysis and intermediate asymptotics*, volume 14. Cambridge University Press, 1996.

[3] Garrett Birkhoff and Jack Kotik. Note on the heat equation. *Proceedings of the American Mathematical Society*, 5(1):162–167, 1954.

[4] Claude Brezinski and Luc Wuytack. *Numerical analysis: Historical developments in the 20th century*. Elsevier, 2012.

[5] George Casella and Roger L Berger. Statistical inference, duxbury press. *Pacific Grove, CA.[Google Scholar]*, 2002.

[6] Pafnutii Lvovich Chebyshev. Des valeurs moyennes. *J. Math. Pures Appl*, 12(2):177–184, 1867.

[7] John Crank. *The mathematics of diffusion*. Oxford university press, 1979.

[8] Cameron Davidson-Pilon. lifelines: survival analysis in python. *Journal of Open Source Software*, 4(40):1317, 2019.

[9] Frederik Michel Dekking, Cornelis Kraaikamp, Hendrik Paul Lopuhaä, and Ludolf Erwin Meester. *A Modern Introduction to Probability and Statistics: Understanding why and how*. Springer Science & Business Media, 2005.

[10] *NIST Digital Library of Mathematical Functions*. http://dlmf.nist.gov/, Release 1.0.26 of 2020-03-15. F. W. J. Olver, A. B. Olde Daalhuis, D. W. Lozier, B. I. Schneider, R. F. Boisvert, C. W. Clark, B. R. Miller, B. V. Saunders, H. S. Cohl, and M. A. McClain, eds.

[11] Temple H Fay and P Hendrik Kloppers. The gibbs' phenomenon for fourier-bessel series. *International Journal of Mathematical Education in Science and Technology*, 34(2):199–217, 2003.

[12] P Gilkey, K Kirsten, and Jh Park. Heat content asymptotics for operators of laplace type with neumann boundary conditions. In *Math. Z.* Citeseer, 1994.

[13] Godfrey Harold Hardy and Marcel Riesz. *The general theory of Dirichlet's series*. Courier Corporation, 2013.

[14] Pavol Kalinay, Ladislav Šamaj, and IGOR TRAVĚNEC. Survival probability (heat content) and the lowest eigenvalue of dirichlet laplacian. *International Journal of Modern Physics B*, 25(15):1993–2007, 2011.

[15] Sidney Redner. *A guide to first-passage processes*. Cambridge University Press, 2001.

[16] M Van den Berg. Heat content and brownian motion for some regions with a fractal boundary. *Probability theory and related fields*, 100(4):439–456, 1994.

[17] Nicolaas Godfried Van Kampen. *Stochastic processes in physics and chemistry*, volume 1. Elsevier, 1992.

[18] Pauli Virtanen, Ralf Gommers, Travis E. Oliphant, Matt Haberland, Tyler Reddy, David Cournapeau, Evgeni Burovski, Pearu Peterson, Warren Weckesser, Jonathan Bright, Stéfan J. van der Walt, Matthew Brett, Joshua Wilson, K. Jarrod Millman, Nikolay Mayorov, Andrew R. J. Nelson, Eric Jones, Robert Kern, Eric Larson, CJ Carey, İlhan Polat, Yu Feng, Eric W. Moore, Jake Vand erPlas, Denis Laxalde, Josef Perktold, Robert Cimrman, Ian Henriksen, E. A. Quintero, Charles R Harris, Anne M. Archibald, Antônio H. Ribeiro, Fabian Pedregosa, Paul van Mulbregt, and SciPy 1. 0 Contributors. SciPy 1.0: Fundamental Algorithms for Scientific Computing in Python. *Nature Methods*, 17:261–272, 2020.

[19] George Neville Watson. *A treatise on the theory of Bessel functions*. Cambridge university press, 1995.